

Contract No:

This document was prepared in conjunction with work accomplished under Contract No. DE-AC09-08SR22470 with the U.S. Department of Energy (DOE) Office of Environmental Management (EM).

Disclaimer:

This work was prepared under an agreement with and funded by the U.S. Government. Neither the U. S. Government or its employees, nor any of its contractors, subcontractors or their employees, makes any express or implied:

- 1) warranty or assumes any legal liability for the accuracy, completeness, or for the use or results of such use of any information, product, or process disclosed; or
- 2) representation that such use or results of such use would not infringe privately owned rights; or
- 3) endorsement or recommendation of any specifically identified commercial product, process, or service.

Any views and opinions of authors expressed in this work do not necessarily state or reflect those of the United States Government, or its contractors, or subcontractors.

Keywords: *Mechanical Properties, Type 304L Stainless Steel, Type 316L Stainless Steel, Type 21-6-9 Stainless Steel, Hydrogen Embrittlement, J-Integral, Helium Embrittlement, High-Energy-Rate Forging, Mechanical Press, Hydraulic Press, Screw Pres, Fusion Welds, Heat-Affected Zone*

Retention: *Permanent*

2016 Accomplishments – Tritium Aging Studies on Stainless Steel: Forging Process Effects on the Fracture Toughness Properties of Tritium-Precharged Stainless Steel

MICHAEL J. MORGAN
Materials Science and Technology

Publication Date: January 2017

This document was prepared in conjunction with work accomplished under Contract No. DE-AC09-08SR22470 with the U. S. Department of Energy

Savannah River National Laboratory
Savannah River Nuclear Solutions, LLC
Aiken, SC 29808



Prepared for the U.S. Department of Energy under contract number DE-AC09-08SR22470.

DISCLAIMER

This work was prepared under an agreement with and funded by the U.S. Government. Neither the U.S. Government or its employees, nor any of its contractors, subcontractors or their employees, makes any expressed or implied:

1. Warranty or assumes any legal liability for the accuracy, completeness, or for the use or results of such use of any information, product, or process disclosed; or
2. Representation that such use or results of such use would not infringe privately owned rights; or
3. Endorsement or recommendation of any specifically identified commercial product, process, or service.

Any views and opinions of authors expressed in this work do not necessarily state or reflect those of the United States Government, or its contractors, or subcontractors.

Printed in the United States of America

**Prepared for
U.S. Department of Energy**

2016 Accomplishments – Forging Process Effects on the Fracture Toughness Properties of Tritium-Precharged Stainless Steel

CONTENTS	PAGE
List of Figures	ii
List of Tables	iv
I. Summary	1
II. Introduction	1
III. Experimental Procedure	2
IV. Experimental Results – Forging Process Effects	8
V. Results –Weld Heat Affected Zones	14
VI. Discussion	18
VII. Conclusions	19
VIII. Future Work	20
IX. Acknowledgements	20
X. References	20
Appendix	22

List of Figures	Page
Figure 1. Shape and Dimensions of Fracture-Toughness Specimen in Millimeters.	4
Figure 2. Forging Process Flow Diagram Showing Four Forging Processes and Three Forging Temperatures: Hydraulic-Press, Mechanical-Press, Screw-Press, and High-Energy-Rate Forging (9).	5
Figure 3. Product of each step for 304L Stainless Steel: (a) Billet Prepared for First Extrusion; (b) After First Extrusion; (c) After Second Extrusion; and (d) After Final Forging (9).	5
Figure 4. Center Section of Final Forged Billet Used For: (a) Hardness Profile and Grain Flow (23) and (b) Arc-Shaped Fracture Toughness Specimens.	6
Figure 5. (a) Mechanical Testing Machine with Environmental Chamber For Non-Charged and Hydrogen-Charged Specimens. (b) Fracture-Toughness Specimen with Crack Length DC Potential Drop Leads and Thermocouple.	7
Figure 6. Typical J-R Curves for As-received (Not Charged), Hydrogen Pre-charged, and Tritium Pre-charged Type 21-6-9 Stainless Steels. J_Q Values Shown Were Determined from the Intercept of the J-R Curve with the 0.2 mm Offset Line. (12).	8
Figure 7. J-R Behavior for Screw Press Type 304L Austenitic Stainless Steel in the As-Forged and Tritium-Precharged Conditions for Two Forging Temperatures: (a) 816°C; and (b) 871°C. Similar Behavior Was Observed for Mechanical Press, Hydraulic Press, and High-Energy-Rate Forgings.	9
Figure 8. Fracture Toughness Values as a Function of Yield Strength for all Specimens Before and After Tritium Precharging and Aging.	10
Figure 9. Average Fracture Toughness Values as a Function of Decay Helium Content for Each of the Four Forgings: (a) 816°C; and (b) 871°C.	11
Figure 10. Fracture Modes for High-Energy-Rate Forged Specimens at 816°C: Not charged (Upper Pair) and (b) Tritium Precharged (Lower Pair).	12

List of Figures (continued)	Page
Figure 11. Fracture Modes for Mechanical Press Specimens at 816°C: Not charged (Upper Pair) and (b) Tritium Precharged (Lower Pair).	13
Figure 12. Fracture Modes for Hydraulic Press Specimens at 816°C: Not charged (Upper Pair) and (b) Tritium Precharged (Lower Pair).	13
Figure 13. Fracture Modes for Screw Press Specimens at 816°C: Not charged (Upper Pair) and (b) Tritium Precharged (Lower Pair).	14
Figure 14. Stainless Steel Welded Rings: (a) 21-6-9 with 308L Filler Metal and (b) 304L with 308L Filler Metal.	15
Figure 15. Type 304L HAZ Specimen Showing Weldment and Notch and Fatigue Pre-crack in Weld HAZ.	15
Figure 16. Three-Point Bend Specimen Testing Configuration Showing Position of Displacement Measurement Gage on Upper Pin and Potential Drop Leads at Specimen Ends and Notch Opening.	18
Figure 17. Typical J-R Behavior for Type 304L Hydrogen-Charged Weld HAZ.	18

List of Tables and Appendix	Page
Table I Composition of Type 304L Austenitic Stainless Steel Forgings (Weight %)	3
Table II Characteristics of Forging Processes, and Resulting Tensile Strength Properties of Forged Material from Ref. (9).	4
Table III - Nominal Strain Rates for Forging Processes (9)	6
Table IV Average Fracture Toughness Values of the As-forged and Tritium-Aged Materials.	10
Table V. Chemical Compositions (wt%) of Base Metal and Filler Metal	15
Table VI Type 304L Stainless Steel Fusion Weld Specimens Crack Tip Location and Exposure Conditions	16
Table VII Type 304L Stainless Steel HAZ Specimens Crack Tip Location and Exposure Conditions	16
Table VIII Type 21-6-9 Stainless Steel Fusion Weld Specimens Crack Tip Location and Exposure Conditions	17
Table IX Type 21-6-9 Stainless Steel HAZ Specimens Crack Tip Location and Exposure Conditions	17
Appendix Poster-Forging Strain Rate and Deformation Temperature Effects on the Fracture Toughness Properties of Type 304L Stainless Steel Precharged with Tritium	22

FORGING PROCESS EFFECTS ON THE FRACTURE TOUGHNESS PROPERTIES OF TRITIUM-PRECHARGED STAINLESS STEEL

I. SUMMARY

Forged austenitic stainless steels are used as the materials of construction for pressure vessels designed to contain tritium at high pressure. These steels are highly resistant to tritium-assisted fracture but their resistance can depend on the details of the forging microstructure. During FY16, the effects of forging strain rate and deformation temperature on the fracture toughness properties of tritium-exposed-and-aged Type 304L stainless steel were studied. Forgings were produced from a single heat of steel using four types of production forging equipment – hydraulic press, mechanical press, screw press, and high-energy-rate forging (HERF). Each machine imparted a different nominal strain rate during the deformation. The objective of the study was to characterize the J-Integral fracture toughness properties as a function of the industrial strain rate and temperature. The second objective was to measure the effects of tritium and decay helium on toughness. Tritium and decay helium effects were measured by thermally precharging the as-forged specimens with tritium gas at 34.5 MPa and 350°C and aging for up to five years at -80°C to build-in decay helium prior to testing. The results of this study show that the fracture toughness properties of the as-forged steels vary with forging strain rate and forging temperature. The effect is largely due to yield strength as the higher-strength forgings had the lower toughness values. For non-charged specimens, fracture toughness properties were improved by forging at 871°C versus 816°C and Screw-Press forgings tended to have lower fracture toughness values than the other forgings. Tritium exposures reduced the fracture toughness values remarkably to fracture toughness values averaging 10-20% of as-forged values. However, forging strain rate and temperature had little or no effect on the fracture toughness after tritium precharging and aging. The result was confirmed by fractography which indicated that fracture modes in the tritium-exposed specimens were similar for all forgings.

Another FY16 objective was to prepare fracture toughness specimens from Types 304L and 21-6-9 stainless steel weldments and heat-affected zones (HAZ) for tritium charging. Four sets of specimens were received from Sandia National Laboratory for fatigue precracking and preliminary testing. The specimens were fabricated by Sandia such that fatigue precracks could be introduced into the steel microstructures of interest: (1) Type of 304L Weldment; (2) Type 21-6-9 Weldment; (3) Type 304L HAZ; and (4) Type 21-6-9 HAZ. Specimens were precracked and a subset returned to Sandia for hydrogen charging and verification testing at SRNL for comparison with earlier Sandia results. The results agreed favorably with Sandia results and the remaining specimens are now scheduled for tritium charging during the third quarter of FY17.

II. INTRODUCTION

Tritium reservoirs are constructed from forged stainless steels and filled and stored at the Savannah River Site. The vessels are constructed from forged stainless steels because of their good compatibility with tritium. These steels are highly resistant to, but not

immune from, the embrittling effects of hydrogen isotopes and helium from tritium decay. Cracking in storage vessels has been observed after extended service times and material properties like ductility, elongation-to-failure, and fracture toughness are reduced with time as tritium and its radioactive decay product, helium, slowly accumulate within the vessel walls during service (1-4).

The effects of tritium on the fracture properties of stainless steels vary with the steel type and microstructure. Typical tritium reservoirs have three main microstructural regions: (1) forged base material; (2) Weldment; and (3) Weld HAZ. Because of tritium aging effects, fracture mechanics properties and steel behavior as a function of tritium and decay helium content in a variety of steel microstructures are needed for fracture modeling, reservoir life prediction, and safety margin evaluations (5– 8).

In this study, the combined effects tritium and forging strain rate, forging temperature, and prior annealing on fracture toughness were investigated in forged Type 304L stainless steel. Forging remnants from an earlier forging study were used (9), which included forgings from four different forging processes that spanned two orders of magnitude in the imposed strain rates during forging. Additionally, the role of forging temperature and annealing prior to the final forging step were considered. Previous work considered the effect of hydrogen precharging on the tensile properties of these forging conditions (10). This study was designed to help answer the question “Which manufacturing process produces the microstructure most resistant to tritium embrittlement effects?”

The fracture mechanics properties of weldments and the HAZ are also of interest. To measure these effects, three-point bend specimens were prepared and initial tests conducted such that the fracture properties of the weldments and HAZ microstructures could be measured as a function of hydrogen, tritium, and decay helium content.

III. EXPERIMENTAL PROCEDURE

The forgings used in this study were obtained from prior work and derived from a single heat of steel (9). The composition of the steel is given in Table I. Switzner et al. (9) had produced forgings to study the effect of forging strain rate and temperature on microstructure and mechanical properties. Forgings of equivalent dimensions were produced by four different forging processes to achieve a range of forging strain rates: Screw press, mechanical (crank) press, hydraulic press, and high-energy-rate forging (HERF). Two different forging temperatures were considered: 816 or 871°C. Additionally, the effect of annealing at a temperature of 954°C prior to the final forging step was also considered. Thus, forgings with 16 unique processing histories were produced: four forging process, each at two final-forging temperatures, and for each temperature, forged with and without a prior annealing step. The forging processes and resulting material properties are summarized in Table II and in more detail in Ref. (9).

In brief, all forging was accomplished with material from the same starting bar of type 304L austenitic stainless steel (102 mm diameter, machined to 95 mm diameter prior to forging). The final forging shape was achieved by a three-step process. The two initial extrusion steps (identical for all forgings) reduced the bar to 59 mm diameter. The final upset-forging step resulted in a forged cylinder with diameter of 71 mm. The rate of forging was varied by using different forging equipment for this final upset-forging step; in

order of increasing deformation rate: (i) Hydraulic; (ii) Mechanical; (iii) Screw; and (iv) HERF. Nominal deformation rates from Ref. (9) are 1, 5, 10, and 100 strain/s for hydraulic, mechanical, screw, and HERF, respectively.

Arc-shaped fracture mechanics specimens shown in Fig. 1 were machined from the center section of the forgings from Switzer et al. (9). The specimens were machined from sections of the final forgings previously used for hardness and grain flow characterization, representing the 16 unique processing histories described above (Fig. 2). Figures 3 and 4 show how the fracture toughness specimens were machined from the final stage billet using sections that were previously used for hardness and grain flow characterization. The available remnants were from billets forged at 816°C and 871°C as well as the billets that were annealed at 954°C prior to the final forging blow.

The specimens were fatigue precracked such that the cracks propagated perpendicular to the cylindrical forging axis (i.e., forging direction) and loaded parallel to the forging axis. Some specimens were pre-charged with tritium at 350°C and 34.5 MPa for 14 days. Decay helium content was developed during storage at -80°C from one to five years prior to testing. The specimen tritium and decay helium concentrations were estimated from the measured decay helium content of a high-energy-rate forged Type 304L specimen given a similar exposure. The tritium exposure conditions are estimated to be sufficient to uniformly saturate the test specimens throughout with a tritium content of approximately 1600 atomic parts per million (appm). Storage at one and five years is estimated to achieve approximately 200 and 600 appm, respectively, of decay helium uniformly distributed in the test specimen. The elastic-plastic J-integral was evaluated for all specimens at ambient temperature by loading to failure at 0.002 mm/s while monitoring load, load-line displacement and crack extension (using a DC potential-drop technique). Two-to-three tests were conducted for each condition and the data were analyzed according to ASTM E1820-99 (11). For all test conditions, the requirements for the uncracked ligament and thickness were not satisfied; therefore, all fracture toughness values are reported as unqualified J_Q values. While all fracture surfaces showed uniform crack fronts, only tritium-exposed specimens showed no evidence of shear lips along the sides of the specimens (implying plane-strain conditions prevailed for these specimens).

Table I Composition of Type 304L Austenitic Stainless Steel Forgings (Weight %)

Fe	Cr	Ni	Mn	Si	C	N	S	P
Bal	19.48	10.69	1.63	0.52	0.029	0.03	0.0064	0.028

Table II Characteristics of Forging Processes, and Resulting Tensile Strength Properties of Forged Material from Ref. (9).

Process	Approximate Strain Rate (s ⁻¹)	Forging Temperature °C	YS (MPa)	UTS (MPa)
Hydraulic	1	816	458	641
Mechanical	5	816	476	649
Screw	10	816	495	656
HERF	100	816	470	651
Screw & Prior Anneal	10	816	483	642
HERF & Prior Anneal	100	816	458	639
Hydraulic	1	871	412	617
Mechanical	5	871	436	628
Screw	10	871	461	631
HERF	100	871	444	637
Prior Anneal + Screw	10	871	461	631
Prior Anneal + HERF	100	871	433	629

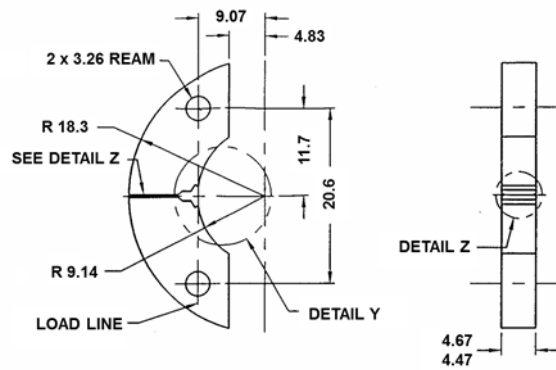


Figure 1. Shape and Dimensions of Fracture-Toughness Specimen in Millimeters.

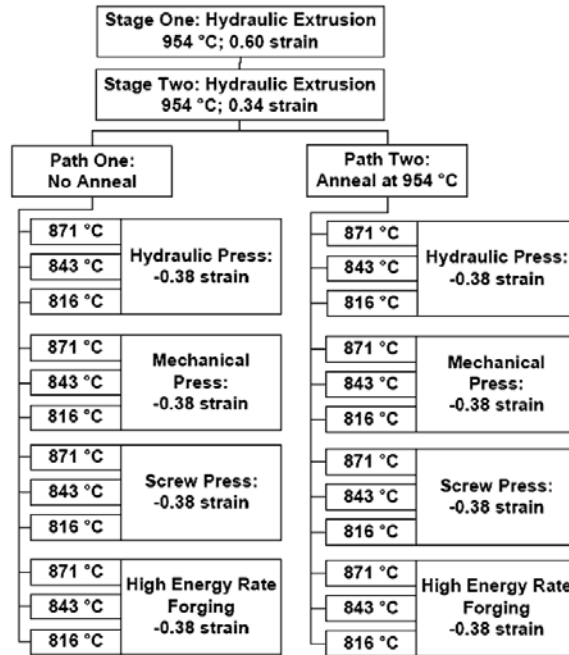


Fig. 1. Flowchart matrix for 304L stainless steel processing experiments.

Figure 2. Forging Process Flow Diagram Showing Four Forging Processes and Three Forging Temperatures: Hydraulic-Press, Mechanical-Press, Screw-Press, and High-Energy-Rate Forging (9).

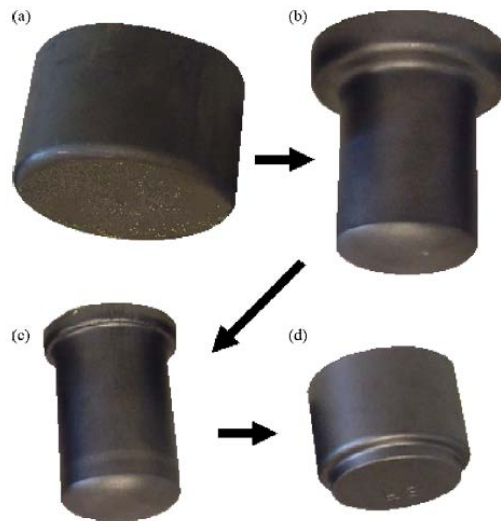


Figure 3. Product of each step for 304L Stainless Steel: (a) Billet Prepared for First Extrusion; (b) After First Extrusion; (c) After Second Extrusion; and (d) After Final Forging (9).

The compositions of the steels are given in Table I. The nominal strain rates for the various forging processes are listed in Table III: Engineering strain rates range from 1 s^{-1} to 125 s^{-1} (9). The size of the remnant section(s) limited the number of specimens that could be fabricated. The test matrix includes fracture toughness measurements on as-forged specimens and two sets of tritium aging conditions.

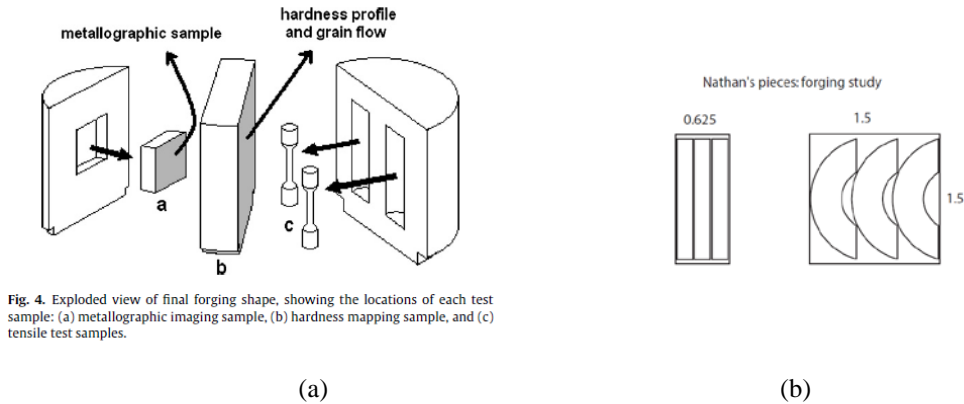


Figure 4. Center Section of Final Forged Billet Used For: (a) Hardness Profile and Grain Flow (22) and (b) Arc-Shaped Fracture Toughness Specimens.

Table III Nominal Strain Rates for Forging Processes (9)

Forging Process	Approximate Forging Die Contact Velocity (mm/s)	Deformation Time (s)	Engineering Strain Rate (s^{-1})
Hydraulic Press	60	0.4	1
Mechanical Press	300	0.08	5
Screw Press	500-575	0.04-0.05	8-10
HERF	5600-7500	0.003-0.005	80-125

J-integral tests were conducted at room temperature in air using a screw-driven testing machine and a crosshead speed of 0.002 mm/s while recording load, load-line displacement with a gage clipped to the crack mouth, and crack length (Figure 5). Crack

length was monitored using a DC potential drop system and guidelines described in the ASTM standard (11). The J-Integral versus crack length increase (J-R) curves were constructed from the data using ASTM E1820-99 (11). Fracture toughness values are determined by using the intercept of an offset line with the J-R curve as shown in Figure 14 which shows data on the effect of tritium from an earlier study (12). The offset line has a slope that is proportional to the flow strength of the material. As the material yields before cracking the crack tip blunts and changes shape. In effect, the ASTM procedure is determining the point at which the crack begins to grow after blunting has occurred. The slope of the blunting line in the standard is generally taken to be between $4/3$ and 2 times the material's flow strength based on best fits to numerous alloys. The flow strength is defined as the average between yield and ultimate strengths. This study included materials having a range of flow strengths with an overall average of 80 ksi. The best-fit slope was $(2.2 \times \text{Flow Strength})$. These best-fit values were used to determine fracture-toughness values to avoid later complications in the analysis because hydrogen, tritium, and decay helium all affect flow strength, and tensile specimens would not be available for each condition. The blunting lines are shown for the J-R Curve results to show the goodness of fit to the data. No attempt was made at this time to quantify the fracture toughness differences as a function of blunting-line slope. In general, fracture toughness values determined with steeper sloped blunting lines are lower and therefore, more conservative. In these high work-hardenable stainless steels, the J-R curve clearly deviates away from the lower sloped blunting lines as the material in front of the crack work hardens prior to crack extension. Because of this, the fracture toughness properties reported here should be conservative.

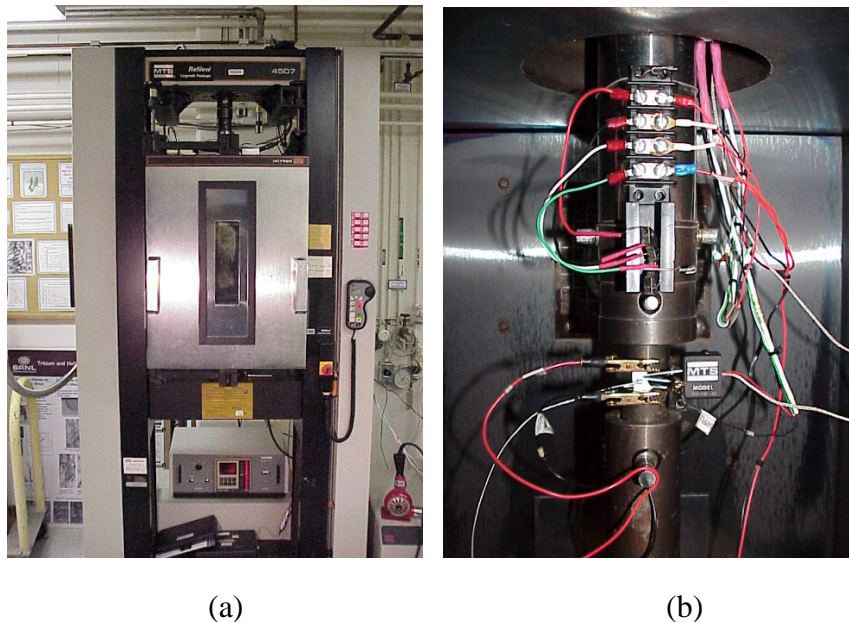


Figure 5. (a) Mechanical Testing Machine with Environmental Chamber For Non-Charged and Hydrogen-Charged Specimens. (b) Fracture-Toughness Specimen with Crack Length DC Potential Drop Leads and Thermocouple.

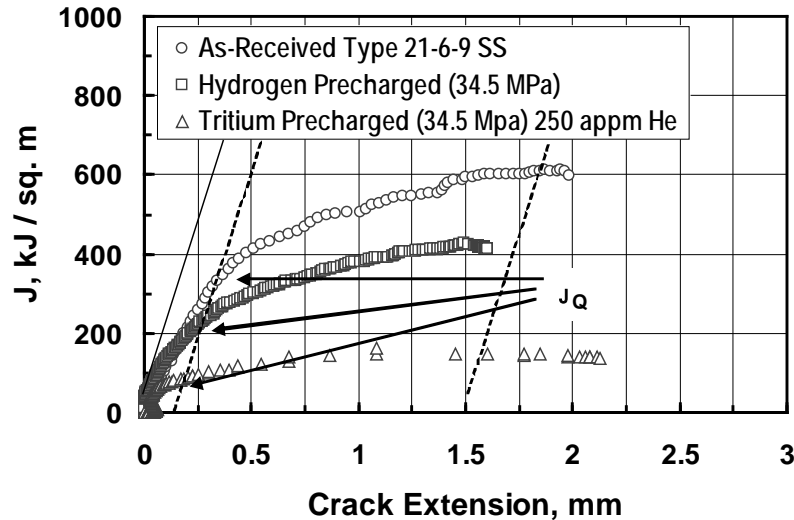
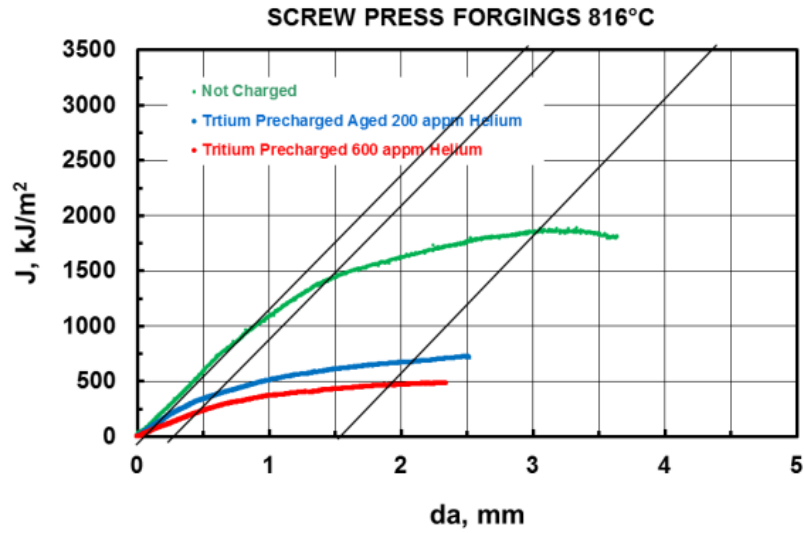


Figure 6. Typical J-R curves for As-received (Not Charged), Hydrogen Pre-charged, and Tritium Pre-charged Type 21-6-9 Stainless Steels. J_Q Values Shown Were Determined from the Intercept of the J-R Curve with the 0.2 mm Offset Line (12).

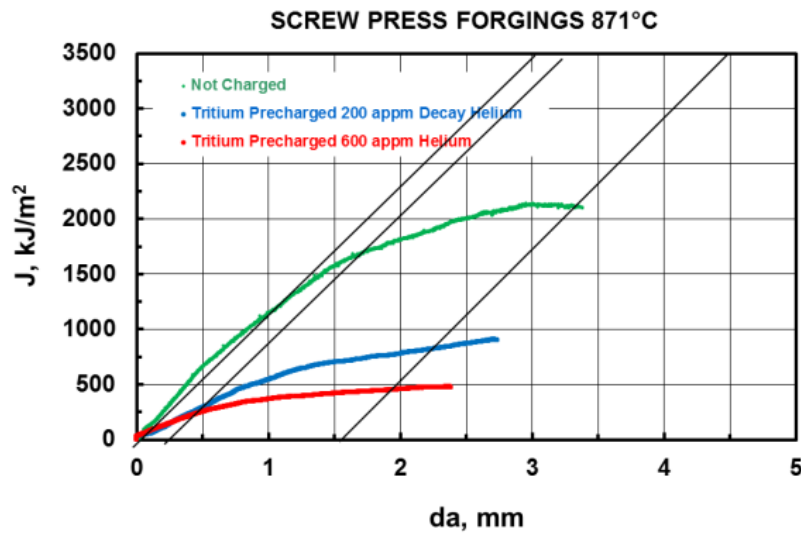
IV. EXPERIMENTAL RESULTS – FORGING PROCESS EFFECTS

Typical J-R (fracture toughness, J vs. change in crack length, da) curves for the screw press forging process conducted at two temperatures are shown in Figure 7. The fracture toughness value, J_Q , is given by the intersection of the J-R curve with the 0.2 mm offset line. In general, specimens forged at 816°C had slightly lower toughness values than those forged at 871°C. The J-R curves are steeper for as-forged specimens and flatter for tritium/helium precharged specimens. The J-R behavior exhibited in these figures is typical for all of the four forging processes and forging temperatures.

The average J_Q value for each forging condition is provided in Table IV. In general, the fracture toughness properties of the as-forged specimens decreased with increasing yield strength. This trend is shown in Figure 8. The screw press forging process at 816°C had the highest yield strength (495 MPa) and lowest fracture toughness values (1340 kJ/m²) of the as-forged steels. Table IV and Figure 9 show the average fracture toughness values as a function of decay helium content for the different forging processes and at the two forging temperatures. Tritium and decay helium caused fracture toughness values to be reduced by 80-90% compared to the as-forged condition for all of the forging processes, although the lowest average value was still greater than 150 kJ/m².



(a)



(b)

Figure 7. J-R Behavior for Screw Press Type 304L Austenitic Stainless Steel in the As-Forged and Tritium-Precharged Conditions for Two Forging Temperatures: (a) 816°C; and (b) 871°C. Similar Behavior Was Observed for Mechanical Press, Hydraulic Press, and High-Energy-Rate Forgings.

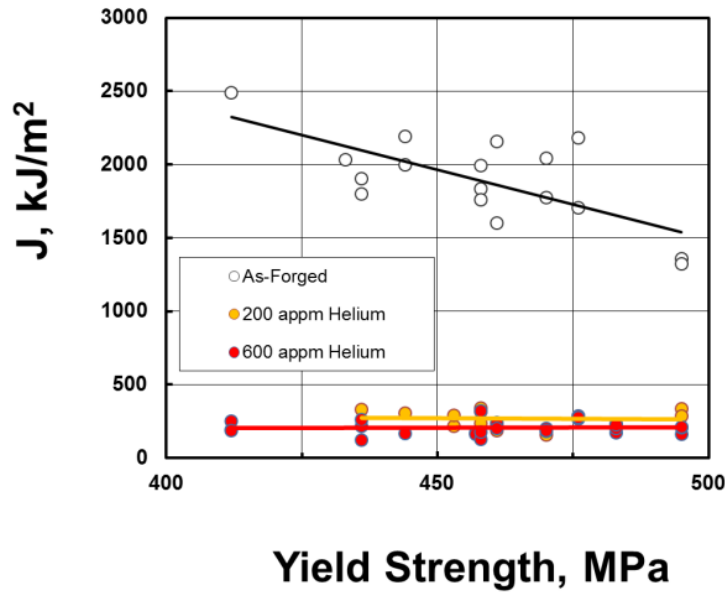
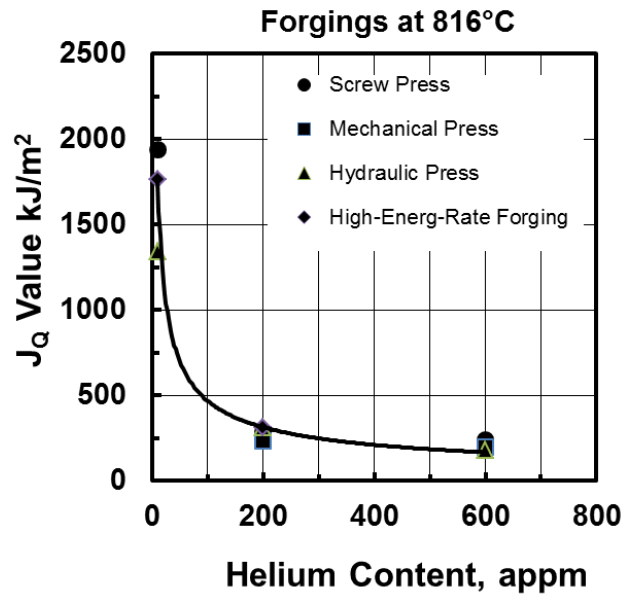


Figure 8. Fracture Toughness Values as a Function of Yield Strength for all Specimens Before and After Tritium Precharging and Aging.

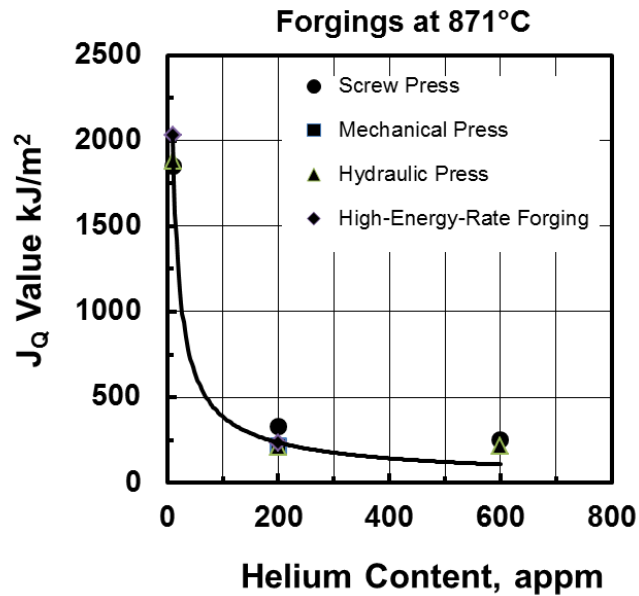
Table IV Average Fracture Toughness Values of the As-Forged and Tritium-Aged Materials.

Process	Forging Temperature (°C)	Fracture Toughness Values, J_Q (kJ/m ²)		
		As-Forged	Decay Helium Content 200 appm (est.)	Decay Helium Content 600 appm (est.)
Hydraulic	816	1915	340	153
Mechanical	816	1940	287	243
Screw	816	1340	309	182
HERF	816	1908	158	209
Prior Anneal + Screw	816	*	233	196
Prior Anneal + HERF	816	2129	216	*
Hydraulic	871	2490	*	229
Mechanical	871	1850	329	252
Screw	871	1880	208	215
HERF	871	2094	307	178
Prior Anneal + Screw	871	*	215	*
Prior Anneal + HERF	871	2031	235	*

*Not measured



(a)



(b)

Figure 9. Average Fracture Toughness Values as a Function of Decay Helium Content for Each of the Four Forgings: (a) 816°C; and (b) 871°C.

Figures 10-13 show the fracture modes that were observed in these steels. For the as-forged steels, the fracture surfaces showed failure by microvoid nucleation and growth processes at the two forging temperatures: (a) 816°C; and (b) 871°C. This is typical for forged steels. There were subtle differences in the average void sizes for different forging processes. For example the Mechanical Press forgings had patches of finer microvoids on their fracture surfaces (Figure 11) while Hydraulic Press forgings had larger microvoids (Figure 12).

Tritium-exposed specimens had different fracture appearance than non-charged specimens. Fracture tended to be characterized by a quasi-cleavage appearance with some twin boundary parting or intergranular failure. Typically, twin boundary parting was isolated (e.g., Figure 13) while the intergranular fracture areas include small patches of two or three grains (e.g., Figure 12). These effects of tritium and decay have commonly been seen and the fracture modes are consistent with the loss in toughness.

A poster was presented at the 2016 International Hydrogen Conference in September of 2016 and is shown in the Appendix. A paper was prepared and submitted to the conference proceedings and is being peer reviewed.

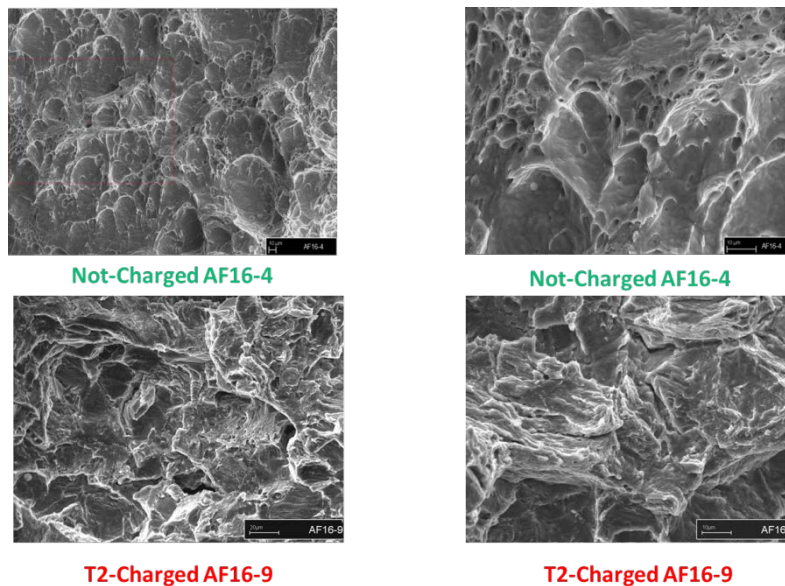


Figure 10. Fracture Modes for High-Energy-Rate Forged Specimens at 816°C: Not charged (Upper Pair) and (b) Tritium Precharged (Lower Pair).

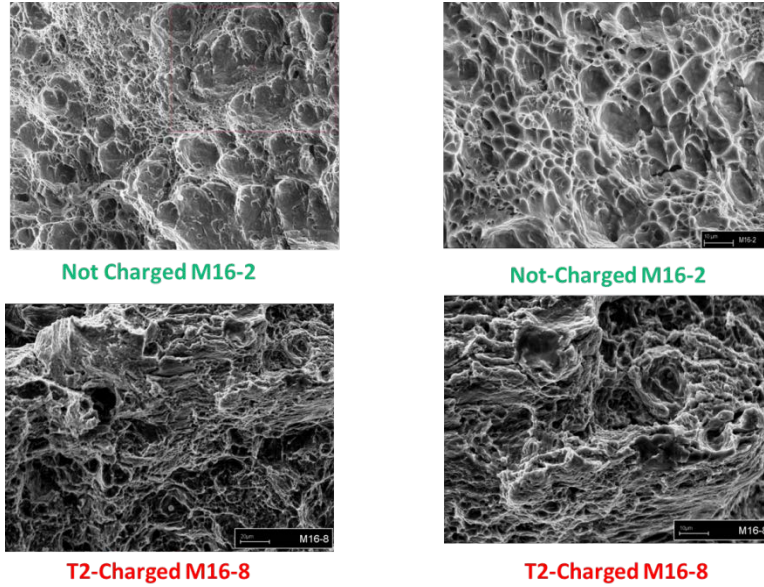


Figure 11. Fracture Modes for Mechanical Press Specimens at 816°C: Not charged (Upper Pair) and (b) Tritium Precharged (Lower Pair).

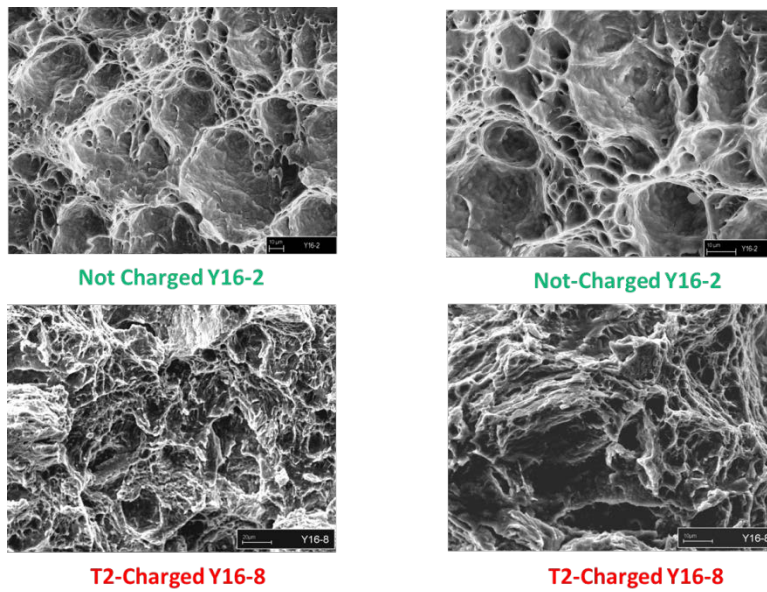


Figure 12. Fracture Modes for Hydraulic Press Specimens at 816°C: Not charged (Upper Pair) and (b) Tritium Precharged (Lower Pair).

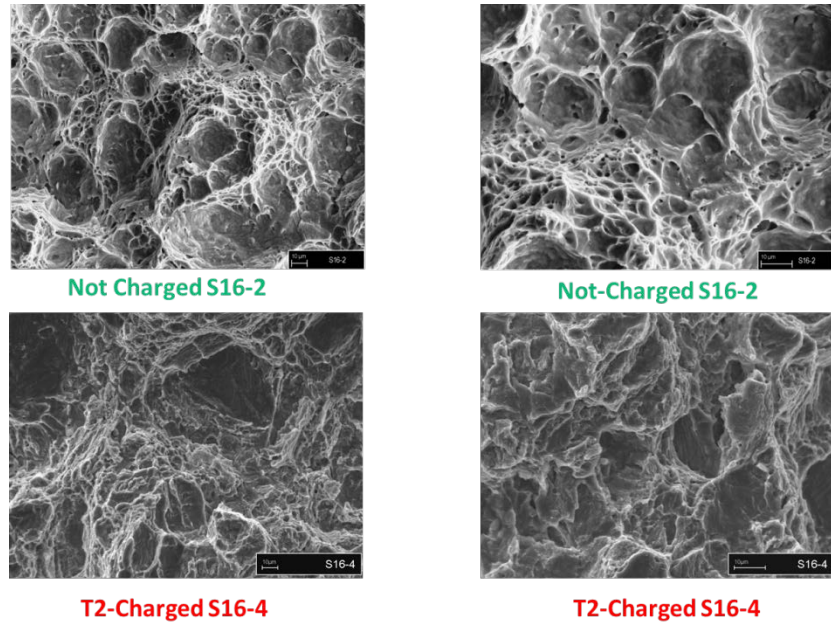


Figure 13. Fracture Modes for Screw Press Specimens at 816°C: Not charged (Upper Pair) and (b) Tritium Precharged (Lower Pair).

V. RESULTS – WELD HEAT AFFECTED ZONES

Table V shows the material compositions for the base metals and filler metals that are being used for the weld heat-affected zone study. The weldments and three-point specimen bend bars were prepared by Sandia National Laboratory. Briefly, three-point bend bars were machined from the weld rings shown in Figure 14. Specimens have been precracked and readied for tritium precharging by SRNL. The specimens will be cleaned and loaded into the tritium charging vessel just prior to the scheduled exposure which is scheduled for 2Q17. Initial tritium tests will be conducted during FY18 and later tests at higher decay helium contents during FY20 and beyond. The specimen test matrix including materials, filler wires, crack locations, and planned exposures are listed in Tables VI through IX.

Figure 15 shows one of the specimens used during a set of round-robin tests with SNL. The specimens had been prepared by SNL with polished surfaces so that fatigue precracking could be carefully monitored and controlled so that the tip of the crack ended up in the microstructure of interest. Round-robin tests were conducted during FY16 to demonstrate successful fatigue cracking procedures and results and that J-integral testing and analysis procedures were consistent between SRNL and SNL.

A set of specimens were returned to SNL for hydrogen precharging and then tested at SRNL. Notched specimens were precracked to a total crack length of 4.75 mm final $K_{\max} < 18.7 \text{ MPa m}^{1/2}$. Specimens were loaded on a screw driven mechanical test frame equipped with a load cell. The 3-pt bend specimen rested between a fixed center pin on top and two support pins on the bottom at a spacing, S , equal to 4 times the specimen width. Spacing was set at 38.1 mm (1.5 in) for current specimen geometry and pin diameters were 6.4 mm (0.25 in). A single-armed displacement gage was attached to the

moving upper pin to monitor displacement. The testing configuration is shown in Figure 16. A typical J-R result is shown in Figure 17. The data were reviewed with SNL and agreed favorably with those previously acquired at SNL.

Table V Chemical Compositions (wt%) of Base Metal and Filler Metal

Material	Fe	Cr	Ni	Mn	Si	C	N	P	S
304L	Bal.	19.38	10.44	1.72	0.57	0.027	0.02	0.021	0.002
21-6-9	Bal.	21.06	7.16	9.11	0.53	0.031	0.28	0.015	0.001
308L Filler	Bal.	20.5	10.3	1.56	0.50	0.028	0.055	0.006	0.012



Figure 14. Stainless Steel Welded Rings: (a) 21-6-9 with 308L Filler Metal and (b) 304L with 308L Filler Metal.

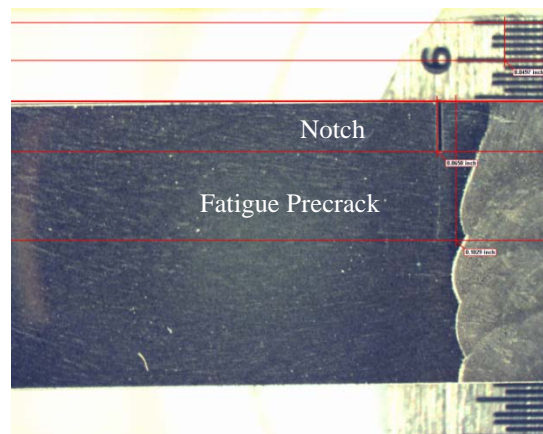


Figure 15. Type 304L HAZ Specimen Showing Weldment and Notch and Fatigue Precrack in weld HAZ.

Table VI Type 304L Stainless Steel Fusion Weld Specimens
Crack Tip Location and Exposure Conditions

Specimen	Base Material	Filler Material	Crack Tip Location	Exposure Conditions		Aging Time, months
FZ-1	304L	308L	Fusion Zone	None	-	-
FZ-2	304L	308L	Fusion Zone	None	-	-
FZ-3	304L	308L	Fusion Zone	Hydrogen	35 MPa; 350°C	-
FZ-4	304L	308L	Fusion Zone	Hydrogen	35 MPa; 350°C	-
FZ-5	304L	308L	Fusion Zone	Tritium	35 MPa; 350°C	3
FZ-6	304L	308L	Fusion Zone	Tritium	35 MPa; 350°C	3
FZ-7	304L	308L	Fusion Zone	Tritium	35 MPa; 350°C	9
FZ-8	304L	308L	Fusion Zone	Tritium	35 MPa; 350°C	9
FZ-9	304L	308L	Fusion Zone	Tritium	35 MPa; 350°C	9
FZ-10	304L	308L	Fusion Zone	Tritium	35 MPa; 350°C	18
FZ-11	304L	308L	Fusion Zone	Tritium	35 MPa; 350°C	18
FZ-12	304L	308L	Fusion Zone	Tritium	35 MPa; 350°C	18
FZ-13	304L	308L	Fusion Zone	Tritium	35 MPa; 350°C	36
FZ-14	304L	308L	Fusion Zone	Tritium	35 MPa; 350°C	36
FZ-15	304L	308L	Fusion Zone	Tritium	35 MPa; 350°C	36

Table VII Type 304L Stainless Steel HAZ Specimens
Crack Tip Location and Exposure Conditions

Specimen	Base Material	Filler Material	Crack Tip Location	Exposure Conditions		Aging Time, months
A-5	304L	308L	HAZ	None	-	-
A-6	304L	308L	HAZ	None	-	-
A-7	304L	308L	HAZ	Hydrogen	35 MPa; 350°C	-
A-8	304L	308L	HAZ	Hydrogen	35 MPa; 350°C	-
A-9	304L	308L	HAZ	Tritium	35 MPa; 350°C	3
A-10	304L	308L	HAZ	Tritium	35 MPa; 350°C	3
A-11	304L	308L	HAZ	Tritium	35 MPa; 350°C	3
A-12	304L	308L	HAZ	Tritium	35 MPa; 350°C	9
A-13	304L	308L	HAZ	Tritium	35 MPa; 350°C	9
A-14	304L	308L	HAZ	Tritium	35 MPa; 350°C	9
A-15	304L	308L	HAZ	Tritium	35 MPa; 350°C	18
A-16	304L	308L	HAZ	Tritium	35 MPa; 350°C	18
A-17	304L	308L	HAZ	Tritium	35 MPa; 350°C	18
A-18	304L	308L	HAZ	Tritium	35 MPa; 350°C	36
A-19	304L	308L	HAZ	Tritium	35 MPa; 350°C	36

Table VIII Type 21-6-9 Stainless Steel Fusion Weld Specimens
Crack Tip Location and Exposure Conditions

Specimen	Base Material	Filler Material	Crack Tip Location	Exposure Conditions		Aging Time, months
9-FZ-1	21-6-9	308L	Fusion Zone	None	-	-
9-FZ-2	21-6-9	308L	Fusion Zone	None	-	-
9-FZ-3	21-6-9	308L	Fusion Zone	Hydrogen	35 MPa; 350°C	-
9-FZ-4	21-6-9	308L	Fusion Zone	Hydrogen	35 MPa; 350°C	-
9-FZ-5	21-6-9	308L	Fusion Zone	Tritium	35 MPa; 350°C	3
9-FZ-6	21-6-9	308L	Fusion Zone	Tritium	35 MPa; 350°C	3
9-FZ-7	21-6-9	308L	Fusion Zone	Tritium	35 MPa; 350°C	9
9-FZ-8	21-6-9	308L	Fusion Zone	Tritium	35 MPa; 350°C	9
9-FZ-9	21-6-9	308L	Fusion Zone	Tritium	35 MPa; 350°C	9
9-FZ-10	21-6-9	308L	Fusion Zone	Tritium	35 MPa; 350°C	18
9-FZ-11	21-6-9	308L	Fusion Zone	Tritium	35 MPa; 350°C	18
9-FZ-12	21-6-9	308L	Fusion Zone	Tritium	35 MPa; 350°C	18
9-FZ-13	21-6-9	308L	Fusion Zone	Tritium	35 MPa; 350°C	36
9-FZ-14	21-6-9	308L	Fusion Zone	Tritium	35 MPa; 350°C	36
9-FZ-15	21-6-9	308L	Fusion Zone	Tritium	35 MPa; 350°C	36

Table IX Type 21-6-9 Stainless Steel HAZ Specimens
Crack Tip Location and Exposure Conditions

Specimen	Base Material	Filler Material	Crack Tip Location	Exposure Conditions		Aging Time, months
B-1	21-6-9	308L	HAZ	None	-	-
B-2	21-6-9	308L	HAZ	None	-	-
B-3	21-6-9	308L	HAZ	Hydrogen	35 MPa; 350°C	-
B-4	21-6-9	308L	HAZ	Hydrogen	35 MPa; 350°C	-
B-5	21-6-9	308L	HAZ	Tritium	35 MPa; 350°C	3
B-6	21-6-9	308L	HAZ	Tritium	35 MPa; 350°C	3
B-7	21-6-9	308L	HAZ	Tritium	35 MPa; 350°C	3
B-8	21-6-9	308L	HAZ	Tritium	35 MPa; 350°C	9
B-9	21-6-9	308L	HAZ	Tritium	35 MPa; 350°C	9
B-10	21-6-9	308L	HAZ	Tritium	35 MPa; 350°C	18
B-11	21-6-9	308L	HAZ	Tritium	35 MPa; 350°C	18
B-12	21-6-9	308L	HAZ	Tritium	35 MPa; 350°C	18
B-13	21-6-9	308L	HAZ	Tritium	35 MPa; 350°C	36
B-14	21-6-9	308L	HAZ	Tritium	35 MPa; 350°C	36
B-15	21-6-9	308L	HAZ	Tritium	35 MPa; 350°C	36

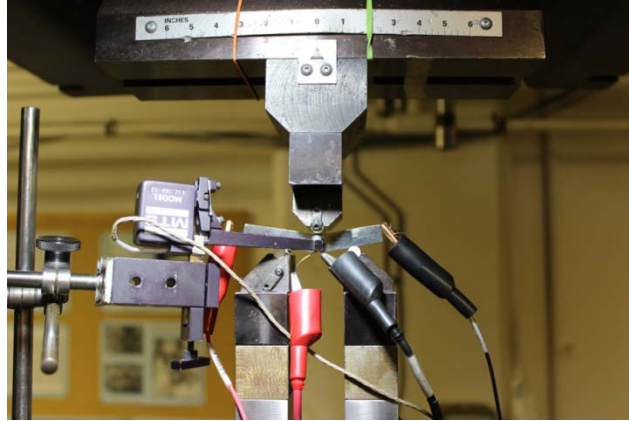


Figure 16. Three-Point Bend Specimen Testing Configuration Showing Position of Displacement Measurement Gage on Upper Pin and Potential Drop Leads at Specimen Ends and Notch Opening.

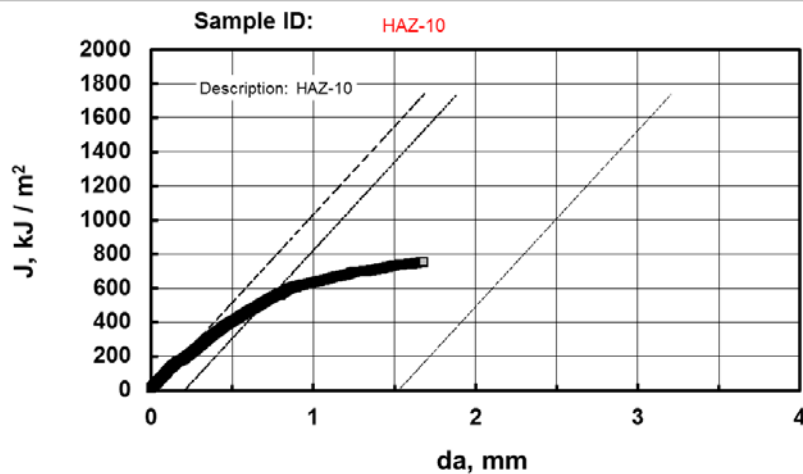


Figure 17. Typical J-R Behavior for Type 304L Hydrogen-Charged Weld HAZ.

VI. DISCUSSION

One of the objectives of this study was to measure the fracture toughness properties of Type 304L stainless steel as a function of forging temperature and forging deformation rate after tritium precharging and aging. Clear trends with these processing characteristics, however, did not emerge from these results. The higher forging temperature generally resulted in greater fracture toughness, although this was not always the case and likely represents scatter in the measurements. There is also no clear trend with forging rate for any of the measured conditions. Similarly, the role of annealing prior to the final stage of forging is inconclusive. Therefore, we consider the values in

Table IV collectively (i.e., independent of the processing characteristics): the average fracture toughness (J_Q) of the as-forged material is more than 1900 kJ/m^2 with a standard deviation of about 300 kJ/m^2 . The material aged for one year (200 appm He) displayed a fracture toughness of $\sim 260 \pm 60 \text{ kJ/m}^2$, while the material aged for five years is $\sim 200 \pm 30 \text{ kJ/m}^2$.

Tritium-precharging produced a significant reduction in the fracture toughness values for all of the materials. The magnitude of the observed reduction is consistent with earlier studies on tritium effects on toughness (4-8). There appears to be a steep decrease in fracture resistance with moderate amounts of helium content, although the baseline fracture resistance with tritium in the absence of helium is not known. Comparison with published results on hydrogen-precharged forged Type 304L stainless steel suggests that the contribution of decay helium to toughness degradation is relatively small in relationship to the contribution of the hydrogen isotope. For example, fracture toughness of similarly forged Type 304L is reported (13) to be nominally in the range of 200-300 kJ/m^2 . (with about twice as much precharged hydrogen based on solubility predictions from Ref. (14) and with much larger specimens). In this study, the tritium content is decreasing as the helium content is increasing and the change in tritium content after one year and five years of aging was not measured. Nevertheless, extrapolation of the modest slope of the J_Q values at high helium content to zero helium content results in about 300 kJ/m^2 , consistent with the forged and hydrogen-precharged Type 304L from Ref (13) and suggesting that the decrease of J_Q can be attributed primarily to tritium.

VII. CONCLUSIONS

- Screw press forging process at 816°C had the highest yield strength (495 MPa) and lowest fracture toughness values (1340 kJ/m^2) for the as-forged steels.
- The fracture toughness values of the mechanical press, hydraulic press, and HERF processes were very high and averaged more than 1900 kJ/m^2 .
- Forging strain rate and temperature had no clear effect on fracture toughness properties after tritium exposures. Collectively for all conditions, J_Q values averaged $\sim 270 \text{ kJ/m}^2$ and 200 kJ/m^2 for 200 and 600 appm decay helium respectively.
- Tritium exposures reduced the fracture toughness by 80-90% compared to the as-forged condition. The majority of this decrease was attributed to the effect of hydrogen isotopes in the absence of decay helium.
- In general, Tritium and decay helium induced a change in fracture mode from microvoid coalescence to quasi-cleavage and twin-boundary parting though subtle differences were observed.

VIII. FUTURE WORK

Companion specimens that were annealed prior to the final forging blow for the four forging process have been tritium exposed and tests will be completed during FY17. The results from those studies will be contrasted with those in this report. Specimens have also been prepared and tritium charged from Stem, Cup, Block, and Brick forgings from Types 304L, 316L, and 21-6-9 stainless steels. These specimens are also being tested during FY17. Weldments and HAZ specimens of Types 304L and 21-6-9 stainless steels will be tritium precharged during FY17 and tested in FY18-20.

IX. ACKNOWLEDGEMENTS

The forgings used in this study were provided by Nathan Switzner, currently at the Colorado School of Mines and Chris San Marchi and Dorian Balch of Sandia National Laboratories. Nathan conducted earlier studies on the forgings and Chris San Marchi and Dorian Balch conducted hydrogen effects studies on the tensile properties of the forgings. Jim Wilderman assisted in conducting the mechanical tests of the tritium-exposed specimens. Henry Ajo conducted the scanning electron microscopy. Chad Sweeney, Calvin Clamp, Dante Pilgrim, and Ken Imrich made invaluable contributions in preparing tritium charging vessels and tritium charging procedures; conducting specimen recovery; and transporting specimens to SRNL after the tritium charging runs.

XI. REFERENCES

1. G. R. Caskey, Jr., "Hydrogen Effects in Stainless Steels", Hydrogen Degradation of Ferrous Alloys, ed. J. P. Hirth, R. W. Oriani, and M. Smialowski, eds., (Park Ridge, NJ: Noyes Publication, 1985), p. 822.
2. S. L. Robinson, "The Effects of Tritium on The Flow and Fracture of Austenitic Stainless Steels", Hydrogen Effects on Material Behavior, A. W. Thompson and N. R. Moody, eds. (Warrendale, PA: TMS 1989) p. 433.
3. S. L. Robinson and G. J. Thomas, "Accelerated Fracture due to Tritium and Helium in 21-6-9 Stainless Steel", Metall Trans, 22A (1991), 879-885.
4. M.J. Morgan and M.H. Tosten, "Tritium and Decay Helium Effects on the Fracture Toughness Properties of Types 316L, 304L, and 21Cr-6Ni-9Mn Stainless Steels", Hydrogen Effects in Materials, A. W. Thompson and N. R. Moody, eds. (Warrendale, PA: TMS, 1996) p. 873.
5. M.J. Morgan, "Hydrogen Effects on the Fracture Toughness Properties of Forged Stainless Steels", 2008 ASME Pressure Vessels and Piping Division Conference, July 27-31, 2008, Chicago, Illinois USA.
6. M.J. Morgan, "Tritium Aging Effects on the Fracture Toughness Properties of Forged Stainless Steels", Proceedings of the Conference on Materials Innovations in an Emerging Hydrogen Economy, February 24-27, 2008, Cocoa Beach, Florida.

7. M. J. Morgan and M. H. Tosten, "Microstructure and Yield Strength Effects on Hydrogen and Tritium Induced Cracking in HERF Stainless Steel", *Hydrogen Effects on Material Behavior*, N. R. Moody and A. W. Thompson, eds. (Warrendale, PA: TMS, 1990) 447-457.
8. M. J. Morgan and M. H. Tosten, "Tritium and Decay Helium Effects on Cracking Thresholds and Velocities in Stainless Steels", *Fusion Technol*, 39, (2001) 590-595.
9. N.T. Switzner, C.J. Van Tyne, and M.C. Mataya, "Effect of Forging Strain Rate and Deformation Temperature on the Mechanical Properties of Warm-Worked 304L Stainless Steel", *J Mater Processing Technol* 210 (2010) 998-1007.
10. N.T. Switzner, T. Neidt, J. Hollenbeck, J. Knutson, W. Everhart, R. Hanlin, R. Bergen, D. K. Balch, C. San Marchi, "Hydrogen-Assisted Fracture in Forged Type 304L Austenitic Stainless Steel", *Hydrogen-Materials Interactions*, B.P. Somerday, P. Sofronis eds. (New York: ASME 2014) p. 273.
11. ASTM E1820-99 "Standard Test Method for Measurement of Fracture Toughness", *1999 Annual Book of ASTM Standard Volume 3.01 Metals-Mechanical Testing; Elevated and Low-Temperature Tests; Metallography*, American Society for Testing and Materials, 1999.
12. M. J. Morgan, S. L. West, and G. K. Chapman, "Tritium Aging Effects on Fracture Toughness of Type 21-6-9 Stainless Steel", **WSRC-TR-2007-00244**, Savannah River National Laboratory, Washington Savannah River Company, Savannah River Site, Aiken, SC, June 14, 2007.
13. H. Jackson, C. San Marchi, D. Balch, B. Somerday, J. Michael, "Effects of low temperature hydrogen-assisted crack growth in forged 304L austenitic stainless steel", *Metall Mater Trans* 47A (2016) 4334-4350.
14. C. San Marchi, B.P. Somerday, "Permeability, solubility and diffusivity of hydrogen isotopes in stainless steels at high gas pressures", *Intern J Hydrogen Energy* 32 (2007) 100-116.

Appendix

Forging Strain Rate and Deformation Temperature Effects on the Fracture Toughness Properties of Type 304L Stainless Steel Precharged with Tritium

Savannah River National Laboratory We put science to work.™

OPERATED BY SAVANNAH RIVER NUCLEAR SOLUTIONS Michael J. Morgan

Purpose

The purpose of this work was to measure and evaluate the effects of tritium and decay helium on the fracture toughness properties of Type 304L stainless steel forged at different strain rates and temperatures¹.

Experimental Procedure

Pre-cracked fracture mechanics specimens were:

- Fabricated from forging remnants;
- Pre-charged with tritium at 850°C and 34.5 MPa;
- Aged from one to five years to build in helium from tritium decay.
- J-Integral tested at ambient temperature by pulling to failure at 0.002 mm/s while monitoring load, load-line displacement and crack extension.

2016 INTERNATIONAL HYDROGEN

Nucleus of Hydrogen is a Hydrogen Environment

Nominal Strain Rates for Forging Process¹

Final Forging Process	Approximate Forging Velocity (mm/s)	Deformation Time (s)	Engineering Strain Rate (s ⁻¹)
Hydraulic Press	60	0.4	1
Mechanical Press	300	0.08	5
Screw Press	575	0.04	10
Dynapack HERF	6500-7500	0.004	100

Hardness Map for Hydraulic Press Forging

Results

SCREEN PRESS FORGINGS 816°C

FORGINGS AT 816°C

Yield Strengths, MPa

Higher Strength Forgings Had Lower Toughness But Similar Fracture Modes and Tritium Compatibility.

Conclusions

- The Screw Press forging process at 816°C had the highest yield strength (495 Mpa) and lowest fracture toughness values (1340 kJ / sq. m) for the as-forged steels.
- The fracture toughness values of the Mechanical Press, Hydraulic Press, and HERF processes were very high and averaged more than 1900 kJ / sq. m). Fracture toughness was improved for all processes if forged at 871°C (~2100 kJ / sq m).
- Tritium exposures reduced the fracture toughness values remarkably to fracture toughness values averaging 10-20% of as-forged values.
- Forging strain rate and temperature had little or no effect on fracture toughness properties after tritium exposures. For 200 appm decay helium, J₀ values averaged 270 kJ / sq. m; for 600 appm decay helium, J₀ averaged 210 kJ / sq. m.

Fracture Toughness Properties Are Reduced After Tritium Precharging & Aging

Forging Strain Rate and Temperature Had Little or No Effect on Tritium Compatibility

Acknowledgments

¹Effect of forging strain rate and deformation temperature on the mechanical properties of warm-worked 304L stainless steel, Switzer, Van Tyne, Malaysia, Journal of Materials Processing Technology 210 (2010) 998-1007.

The forgings for this work were supplied by Nathan Switzer of Kansas City National Security Campus and Sandia National Laboratory. Chris San Marchi, Dorlan Bakis, and Brian Kormendy of Sandia National Laboratory were instrumental in planning the work and in providing the forging remnants. Jin Wilkman and Glenn Chapman assisted in conducting the fracture toughness tests. Henry Ajo of SRNL conducted the fractography examinations.

SRNL is a U.S. Department of Energy National Laboratory operated by Savannah River Nuclear Solutions.